Materials Today Bio 29 (2024) 101350

Contents lists available at ScienceDirect

Materials Today Bio

journal homepage: www.journals.elsevier.com/materials-today-bio

Decellularized adipose matrix hydrogel-based in situ delivery of antagomiR-150-5p for rat abdominal aortic aneurysm therapy

Xin Chen [a,1], Shoushuai Wang [a,e,1], Weijian Hou [a], Yanhui Zhang [a,1], Yapeng Hou [a,1], Hao Tong [a], Xiaoxin Zhang [a], Yue Liu [a], Ruoxuan Yang [d], Xiang Li [b,**], Qin Fang [c,***], Jun Fan [a,*]

[a] Department of Tissue Engineering, School of Intelligent Medicine, China Medical University, No.77 Puhe Road, Shenyang North New Area, Shenyang, Liaoning Province, 110122, PR China

[b] Department of Cell Biology, School of Life Sciences, China Medical University, No.77 Puhe Road, Shenyang North New Area, Shenyang, Liaoning Province, 110122, PR China

[c] Cardiac Surgery, First Hospital of China Medical University, Shenyang, Liaoning Province, 110001, PR China

[d] Department of Dental Implantology, School and Hospital of Stomatology, China Medical University, Liaoning Provincial Key Laboratory of Oral Diseases, Shenyang, Liaoning Province, PR China

[e] Department of Radiology, Hainan General Hospital, Hainan Affiliated Hospital of Hainan Medical University, Haikou, Hainan Province, 570311, PR China

ARTICLE INFO

Keywords:
Abdominal aortic aneurysm
AntagomiR-150-5p
Inflammation
Hydrogel
Decellularized adipose matrix

ABSTRACT

Abdominal aortic aneurysm (AAA) is a progressive aortic disease featured by inflammation, vascular smooth muscle cells (VSMCs) depletion, and elastin degradation. MicroRNAs were related to AAA formation, which bring the approach for precise and targeted drug therapy for AAA. We developed a new strategy based on decellularized adipose matrix (DAM) hydrogel immobilized on the adventitia to release antagomiR-150-5p for preventing the AAA development. In this study, $CaCl_2$-induced and elastase-induced rat AAA models were established. We found that miR-150-5p was upregulated while Notch3 was downregulated in two rat AAA models. Then a mold was designed for shaping hydrogel for miR-150-5p delivery around the abdominal aorta. Interestingly, inhibition of miR-150-5p in AAA by local release of antagomiR-150-5p with DAM hydrogel significantly prevented aortic dilation and elastin degradation. Moreover, inflammatory cell infiltration, the expression of inflammatory cytokines (MCP-1, TNF-α, and NF-κB (p65)), and matrix metalloproteinases (MMP-2, MMP-9) were increased while Notch3 and α-SMA were decreased in rat AAA, which can be attenuated by antagomiR-150-5p treatment. In VSMCs with TNF-α stimulation, we further demonstrated that inhibition of miR-150-5p downregulated NF-κB (p65), MMP-2, and MMP-9 and upregulated elastin via Notch3. This work presents a translational potential strategy for AAA repair via DAM hydrogel sustained release of antagomiR-150-5p, and highlights the mechanism of miR-150-5p during AAA progression by regulating Notch3.

1. Introduction

AAA is a localized and progressive dilation of the infrarenal aorta. Multiple inflammatory cells infiltration, and excessive pro-inflammatory molecules and chemokines play crucial roles in AAA development[1]. In addition, aortic dilation and eventual rupture are closely related to VSMCs dysfunction and elastin fragmentation [2]. Surgical repair, such as open surgery and endovascular repair, is routinely conducted to treat AAA, which is accompanied by high mortality [3,4]. However, there are no effective pharmacological treatments for AAA.

MicroRNAs are a class of evolutionarily highly conserved short noncoding RNAs with 18–25 nucleotides. They can inhibit their targets by cleaving and degrading target mRNAs or inhibiting protein translation [5]. Recent data highlighted that miR-150 was involved in cardiovascular disease. MiR-150-5p knockdown could attenuate the formation of atherosclerotic plaques and vulnerable plaques by reducing the production of inflammatory cytokines [6]. Our recent work showed that bone marrow cells transplantation from miR-150 knockout mice

* Corresponding author.
** Corresponding author.
*** Corresponding author.
E-mail addresses: cmu_LX@163.com (X. Li), fanqinok@sina.com (Q. Fang), jfan@cmu.edu.cn (J. Fan).
[1] These authors contributed equally to this work.

https://doi.org/10.1016/j.mtbio.2024.101350
Received 22 August 2024; Received in revised form 11 November 2024; Accepted 17 November 2024
Available online 20 November 2024

also attenuated aortic stiffening and hypertension in SAMP1 mice through inhibiting inflammation [7]. These evidences indicated that miR-150-5p might be associated with the development of AAA.

Notch signaling is involved in multiple aspects of vascular development, including angiogenesis, VSMCs differentiation, and vascular remodeling [8]. In adult tissues, Notch3 is predominantly expressed in VSMCs. In the differentiation process of bone marrow-derived monocytes into smooth muscle α-actin positive cells, the level of Notch3 is increased [9]. Whereas, Notch3 deficiency impairs coronary microvascular maturation and reduces cardiac recovery after myocardial ischemia [10]. In addition, the expression of Notch3 was downregulated in AAA [11]. Our recent data showed that Notch3 was the downstream target of miR-150-5p in regulating the adipogenic differentiation of adipose-derived stem cells [12]. However, whether miR-150-5p/Notch3 are involved in the development of AAA is unknown.

The drugs could be delivered to treat the aneurysm models through different methods. The delivery strategies included systemic intravenous injection, intraperitoneal injection, oral gavage, and local application in aneurysm. Local and direct therapy can improve therapeutic efficacy and reduce systemic toxicity. Previous study showed that extravascular administration of drug-loaded hydrogel was a translational potential way for treating AAA [13]. The hydrogel is widely used to fill spaces, and deliver bioactive molecules, drugs, and cells [14–17]. The micro-fracture adipose with a simple freezing/thawing treatment could be effective in adsorbing and releasing large amounts of drug, which was a good natural scaffold for drug delivery [12]. DAM hydrogel is derived from the adipose tissue, which is rich in adipose ECM components, such as collagens, glycosaminoglycans, laminin, elastin, and fibronectin. There exists adipose tissue in the periphery of the abdominal aorta, which is involved in vascular homeostasis [18]. To mimic the niche of the aorta, we hypothesized that the DAM could work as perivascular scaffold for delivery of antagomiR-150-5p to inhibit aortic aneurysm.

In this study, from the translational perspective for AAA reconstructions, we designed a novel injectable DAM hydrogel delivery system to release antagomiR-150-5p around the aorta. We demonstrated the potential of antagomiR-150-5p delivered in DAM hydrogel for the treatment of AAA. We also explored the mechanistic relationship of miR-150-5p and inflammation in the pathogenesis of AAA, with a focus on the regulation of the Notch3 pathway.

2. Materials and methods

2.1. DAM powder preparation

The DAM was prepared based on our previous method [19], the adipose tissues were sheared into pieces and homogenized by a homogenizer. Then the tissue suspension was centrifuged (10,000 rpm, 40 min) to collect the lowest white precipitates. The residual lipid was removed by soaking in 100 % isopropanol. The cellular components were removed by physical freeze-thawing, hypertonicity, and enzymatic treatment. The precipitates were freeze-dried, powdered, and sterilized to obtain the DAM powder. Finally, DAM was stored at -80°C until use.

2.2. Histological and DNA analysis of DAM

Hematoxylin and Eosin (HE) staining, DAPI staining, Oil Red O staining and Masson trichrome staining were used according to the instructions. The residual DNA of DAM was quantified by using the Tissue DNA Extraction Kit (Solarbio, China) following the manufacturer's instructions. 25 mg adipose tissue and DAM were digested with Proteinase K respectively. The DNA contents were measured with a UV VIS spectrophotometer (SHIMADZU, Japan) by absorption at 260 nm.

2.3. DAM hydrogel preparation

To prepare DAM hydrogel, the sterile DAM powder (10 mg/mL) was dissolved in 2 mg/mL sterile pepsin and 0.01 M HCl solution, and stirred fully at 4°C for 48 h until no visible powdery substance was present. The digest solution was adjusted to pH neutral with sterile 0.1 M NaOH and 10 × PBS. Then, the DAM hydrogel was stored at 4°C for further experiment.

2.4. Fourier-Transform Infrared (FTIR) and scanning electron microscopy

The molecular structure of DAM hydrogel was detected by FTIR. The DAM hydrogel was placed at 37°C for 30 min, following by freezing at -80 °C for 24 h and lyophilized 48 h. The dry DAM hydrogel was quenched with liquid nitrogen and sprayed platinum on the surface to visualize its ultrastructure with scanning electron microscopy (Jeol, Japan).

2.5. Sodium dodecylsulfate polyacrylamide gel electrophoresis (SDS-PAGE)

After electrophoresis, the SDS-PAGE gel (Beyotime, China) was washed with deionized water for 5 min to remove the liquid, and then added 20 mL of rapid staining solution of Coomassie Blue (Beyotime, China) and stained for 20 min at room temperature, discarded the staining solution, and then rinsed by adding 50 mL of deionized water, each time for 5 min for 3 times. Finally, images were captured using a gel imager (Tanon, China).

2.6. Rheology

Rheological properties were studied using the MCR 102 rheometer (Anton Paar, Canada) with a 40 mm parallel plate geometry. Temperature sweep experiment was performed from 10°C to 37°C. 1 mL DAM hydrogel was loaded onto the rheometer plate pre-cooled to 10°C. After loading, the storage (G') and loss (G'') moduli were measured by applying a 5% strain at a frequency of 0.5 Hz.

2.7. Cells viability assay of the DAM hydrogel

To clarify the effect of DAM hydrogel on the viability of vascular cells (VSMCs, HUVECs, and L929 fibroblasts), CCK-8 assay and acridine orange (AO) and propidium iodide (PI) staining were performed. Rat aortic VSMCs were obtained as our previous experiment [20], HUVECs were obtained from the American Type Culture Collection (Rockvile, USA), and L929 cells were obtained from the Cell Culture Center, Beijing Institute of Basic Medical Science of the Chinese Academy of Medical Science (Beijing, China). The dry DAM hydrogel was completely immersed in DMEM media (Gibco, USA) or 1640 media (Gibco, USA) supplemented with 10% FBS (Gibco, USA) and 1% penicillin/streptomycin in the incubator (Thermo, USA) at 37°C with 5% CO_2 to acquire the leach liquor (hydrogel: media = 1 mg: 1 mL). Cells were seeded and cultured at a density of 50%–60% in 96-well microplates for 24 h at 37°C. Then, the cells were treated with concentrations of 1 mg/mL leach liquor. After treatment for 1,3,5,7 days, a total volume of 100 μL DMEM containing 10 μL of CCK-8 solution (Biosharp, China) was added to each well and then cultured for 1 h. All experiments were performed in six repetitions. Finally, the absorbance was measured at the wavelength of 450 nm with a microplate reader (Thermo, USA) using wells without cells as blanks. AO/PI staining was performed according to the manufacturer's protocols (Beibo, China). Then, the samples were observed with a fluorescence microscope.

2.8. The DAM hydrogel degradation

The biodegradation of the DAM hydrogel was determined in PBS (pH 7.4) or 1U collagenase solution at 37°C. 100 μL DAM hydrogel was incubated at 37°C for 30 min, following by placed in transwell chamber

containing 1 mL PBS or collagenase solution. At different time intervals, each hydrogel was weighed after all surface water was carefully blotted off.

2.9. Antagomir150-5p distribution, release, and uptake

To observe the distribution of antagomiR-150-5p in the DAM hydrogel, cy5-antagomiR-150-5p (Pharma, China) was mixed with DAM hydrogel and incubated at 37°C for 30 min, and the images were captured using the confocal laser scanning microscope (Nikon AXR, Japan).

DAM hydrogel was loaded with antagomiR-150-5p or PBS, following by incubation at 37°C for 30 min in a 2 mL tube as previous study [21]. 100 μL PBS was added on top of DAM hydrogel. At every indicated point, the PBS was collected and replaced with fresh PBS. The antagomiR-150-5p content of the samples was quantified by measuring the content of RNA at $\lambda = 260$ nm with a Micro UV spectrophotometer (Biodrop, UK).

To determine the amount of antagomiR-150-5p uptake by HUVECs, VSMCs and L929 fibroblasts,1ug Cy5-antagomiR-150 was added to the respective culture medium (6-well plate). At different time points, the cells were fixed in 4% phosphate-buffered paraformaldehyde. DAPI staining were performed to observe cell nucleus. Finally, the cells were visualized and photographed under a fluorescence microscope.

Cy5-antagomiR-150-5p was delivered via DAM hydrogel in vivo to detect its uptake. The abdominal aortas were collected at 6, 12, and 24 h after delivery. Then the aortas were fixed and cut along the longitudinal axis of the lumen, stained with DAPI, and scanned by laser confocal to observe the existence of antagomiR-150-5p.

2.10. Designing the mold of shaping hydrogel

A silicone hose of 2 mm internal diameter (length in 8 mm) was used as the delivery mold for DAM hydrogel. The silicone hose was cut open to create an incision along the longitudinal axis. Then the above prepared mold was sterilized for applying in the rat AAA models to shape the hydrogel around the aorta.

Adult male 8-week-old Wistar rats were used in the AAA models. After separating the abdominal aorta from the inferior vena cava, the prepared silicone hose mold was placed around the abdominal aorta through the incision to shape the hydrogel (Video 1). Then the DAM hydrogel was delivered by a sterile 200 μL pipette tip and implanted into the cavity between the silicone hose and the abdominal aorta (Video 2). Subsequently, the rat was placed in the multifunction incubator (FuYi-Lian, China) at 37°C for 30 min to obtain complete gelling, followed by removing the silicone hose and closing the abdominal cavity in layers. The aorta wrapped by the gel was taken after 1,3,5,7 days. Masson's staining was performed to observe the degradation of DAM hydrogel.

2.11. Animal experiments

All animal experiments were performed in strict accordance with the recommendations of the National Institutes of Health Laboratory Animal Care and Use Guidelines. The program was approved by the Institutional Animal Care and Use Committee of China Medical University. Wistar rats were obtained from HFK Biotechnology (Beijing, China). All rats were housed under a 12h light/dark cycle and were free to access to normal diet and water.

2.12. Rat study protocols

In the first protocol (IACUC Issue No. CMU2021003), adult male 8-week-old Wistar rats were used to establish $Cacl_2$-induced AAA model and elastase-induced AAA model. For each AAA model, all rats were randomly assigned to the normal group (n = 12) and AAA group (n = 12). Rats were anesthetized by intraperitoneal injection of sodium pentobarbital (40 mg/kg) before surgery. For $Cacl_2$-induced AAA model, the gauze soaked in 0.5 M $CaCl_2$ (Solarbio, China) was placed over the abdominal aorta and removed after 15 min. Rat in the normal group received PBS-soaked gauze treatment for 15 min. After 28 days, these rats were sacrificed for aortic tissues collection. Similarly, 4 U elastase (Yuanye, China) was used in the periphery of the abdominal aorta for 30 min to establish the elastase-induced AAA [22]. After 14 days, aortic tissues were also collected for further analysis.

In the second protocol (IACUC Issue No. CMU2021146), the antagomiR-150-5p NC or antagomiR-150-5p were delivered to the AAA via DAM hydrogel in rats. Adult male 8-week-old Wistar rats were randomly divided into five groups, i.e. sham group, AAA group, DAM group (DAM hydrogel), antagomir NC group (DAM hydrogel with antagomiR-150-5p NC), antagomiR-150-5p group (DAM hydrogel with antagomiR-150-5p), 8 rats per group. Two kinds of AAA models ($Cacl_2$-induced AAA model and elastase-induced AAA model) were made, and grouped as above. After AAA models were established, 10 nmol antagomiR-150-5p or antagomiR-150-5p NC (RiboBio, China) was mixed in sterile DAM hydrogel (composite hydrogel) as the previous study [23]. Then the aorta was wrapped by the silicone hose for shaping hydrogel as mentioned above. The composite hydrogel was injected into the space between the periphery of the abdominal aorta of rats and the silicone mold. After 30 min at 37°C, removing the silicone hose (Fig. 3A). All practices were under the asepsis technique. The $Cacl_2$-related rats were sacrificed after 4 weeks to collect aortas for further study. The elastase-related rats were sacrificed after 2 weeks for further study.

2.13. Aneurysm quantification

The aortic diameter in different groups was calculated using SZH light microscopy (Tokyo, Japan) as described previously [20]. In addition, all rats were subjected to 2-dimensional color-coded doppler ultrasound imaging utilizing a Sequoia ultrasound system with a linear array ultrasound transducer (Visual Sonic Vevo3100, Lab).

2.14. Cell culture

Primary rat aortic VSMCs were obtained as our previous experiment [24]. Then VSMCs were cultured in DMEM (Gibco, USA) supplemented with 10% fetal bovine serum (Gibco, USA), 1% streptomycin, and penicillin in a humidified incubator (Thermo, USA) at 37°C with 5% CO_2. The 3rd passage VSMCs were used for experiments. To mimic AAA inflammatory environment, VSMCs were treated with 100 ng/mL TNF-α (Proteintech, China) for 48 h as previous study [25].

miR-150-5p inhibitor, miR-150-5p mimics and their negative control (GenePharma, China) were delivered via LipofectamineTM 3000 reagent (Invitrogen, USA). VSMCs with a knockdown of Notch3 were obtained by shR-Notch3 lentiviral vector (GenePharma, China) transfection. In brief, VSMCs were infected with lentiviral vector for 24 h and cultured with fresh medium for 48 h. Then, 1.5 μg/mL Puromycin Dihydrochloride (Beyotime, China) was used to select cells with stable knockdown of Notch3 (shR-VSMCs) for further experiments.

2.15. RNA isolation and quantitative real-time PCR

Total RNA was extracted from VSMCs and aortic tissues from different rat groups using Trizol (Takara, Japan) according to the manufacturer's instructions. Strand-specific and reverse miR-150-5p primers (RiboBio, China) were used for the reverse transcription of miR-150-5p. Quantitative real-time PCR (qRT-PCR) was performed with the SYBR Premix Ex Taq TM Kit (RiboBio, China) using a Light Cycler 480 II system (Roche Diagnostics, Basel, Switzerland). U6 was used as an internal control to normalize gene expression.

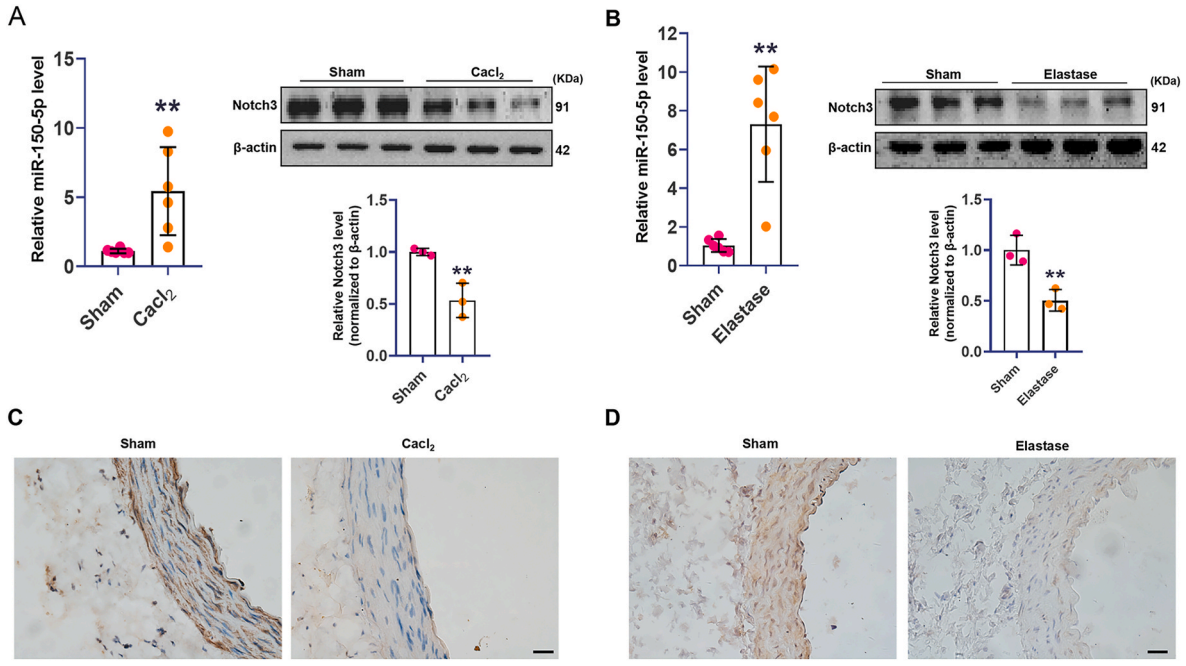

Fig. 1. MiR-150-5p was increased while Notch3 was decreased in AAA. (A). Real-time PCR analysis of miR-150-5p expression, and Western blot analysis of Notch3 expression in aortas in $Cacl_2$-induced rat AAA group and sham group, **p < 0.01 *Vs.* sham group. **(B).** Real-time PCR analysis of miR-150 expression, and Western blot analysis of Notch3 expression in aortas in elastase-induced AAA model and sham group, **p < 0.01 *Vs.* sham group. **(C)**. Representative photomicrographs of Notch3 of immunostaining in $Cacl_2$-induced AAA group and sham group, scale bar, 50 μm. **(D).** Representative photomicrographs of Notch3 of immunostaining in elastase-induced AAA group and sham group, scale bar, 50 μm.

2.16. Histological staining

Samples were fixed in 4% phosphate-buffered paraformaldehyde for 24 h, dehydrated, embedded, and cut into 5 μm slices. Hematoxylin and Eosin (HE) staining and Orcein staining were used according to the instructions. Elastin degradation in the aortas was double-blindly scored according to the following standards: 1, less than 25% degradation; 2, 25%–50% degradation; 3, 50%–75% degradation; 4, greater than 75% degradation.

2.17. Immunohistochemical staining

Aortic tissue was post-fixed in 4% paraformaldehyde, embedded in paraffin, and sectioned at a 5 μm thickness. An immunohistochemical staining kit (Boster, China) was used in this part. Briefly, aortic tissue sections were deparaffinized and hydrated before staining, and endogenous peroxidase activity was blocked with 3% hydrogen peroxide for 10 min at room temperature. Subsequently, bovine serum was performed to block nonspecific binding sites for 30 min at a 37°C incubator. The sections were incubated with antibodies against CD45 (1:300, Bioss, China), CD68 (1:300, Bioss, China), MCP-1 (1:200, Bioss, China), TNF-α (1:100, Absci, USA) and α-SMA (1:300, Bioss, China) overnight at 4°C and then with appropriate secondary antibodies conjugated with HRP at room temperature for 60 min. The phosphate buffer solution (PBS) was used instead of the primary antibody for a negative control experiment. 3,3′- diaminobenzidine (DAB) was used for subsequent color rendering (brown color on positives). Slides were counterstained with hematoxylin. The images were obtained via the upright microscope (Olympus, Japan).

2.18. Western blot

VSMCs and aortic tissues were harvested and lysed in RIPA assay buffer (Beyotime, China) containing the 1% protease inhibitors (Beyotime, China) and 1% phosphatase inhibitors (Beyotime, China). Total lysates are collected in the EP tubes, crushed by 3 s ultrasound at 5 s intervals for 3 times, placed 2 h on ice, and centrifuge at 4°C, 12000 rpm 30 min. Protein concentrations were determined using a BCA Protein Assay Kit (Beyotime, China). Denatured proteins were separated via electrophoresis and transferred to 0.45 μm poly-vinylidene fluoride (PVDF) membranes (GE Amersham, USA) via Trans-Blot (Tanon, China). Membranes were incubated with primary antibodies for 14-16 h at 4°C after being blocked by non-fat milk (5%, w/v) for 2 h at room temperature, and were incubated with secondary antibodies for 2 h at room temperature. Ultimately, membranes were sensed with Tanon™ ECL Western Blotting Substrate (Tanon, China). The automatic chemiluminescence image analysis system (Tanon, China) was used to acquire images. Image J software (National Institutes of Health, USA) was used to analyze quantificationally. In this study, anti-Notch3 (1:1000, CST, USA), anti-elastin (1:1000, ABclonal, China), anti-NF-κB (p65) (1:1000, Bioss, China), anti-MMP-2 (1:1000, ABclonal, China), anti-MMP-9 (1:1000, ABclonal, China), anti-β-actin (1:5000, Bioss, China) were used.

2.19. Statistical analysis

Data were analyzed using prism software and are presented as the mean ± standard deviation (SD). A normal distribution test was performed for all continuous variables. After the confirmation of equal variance among groups, comparisons between two groups were performed with independent-sample t-tests, and comparisons among three or more groups were performed with one-way analysis of variance (ANOVA) followed by Bonferroni's tests. P value < 0.05 indicated statistical significance.

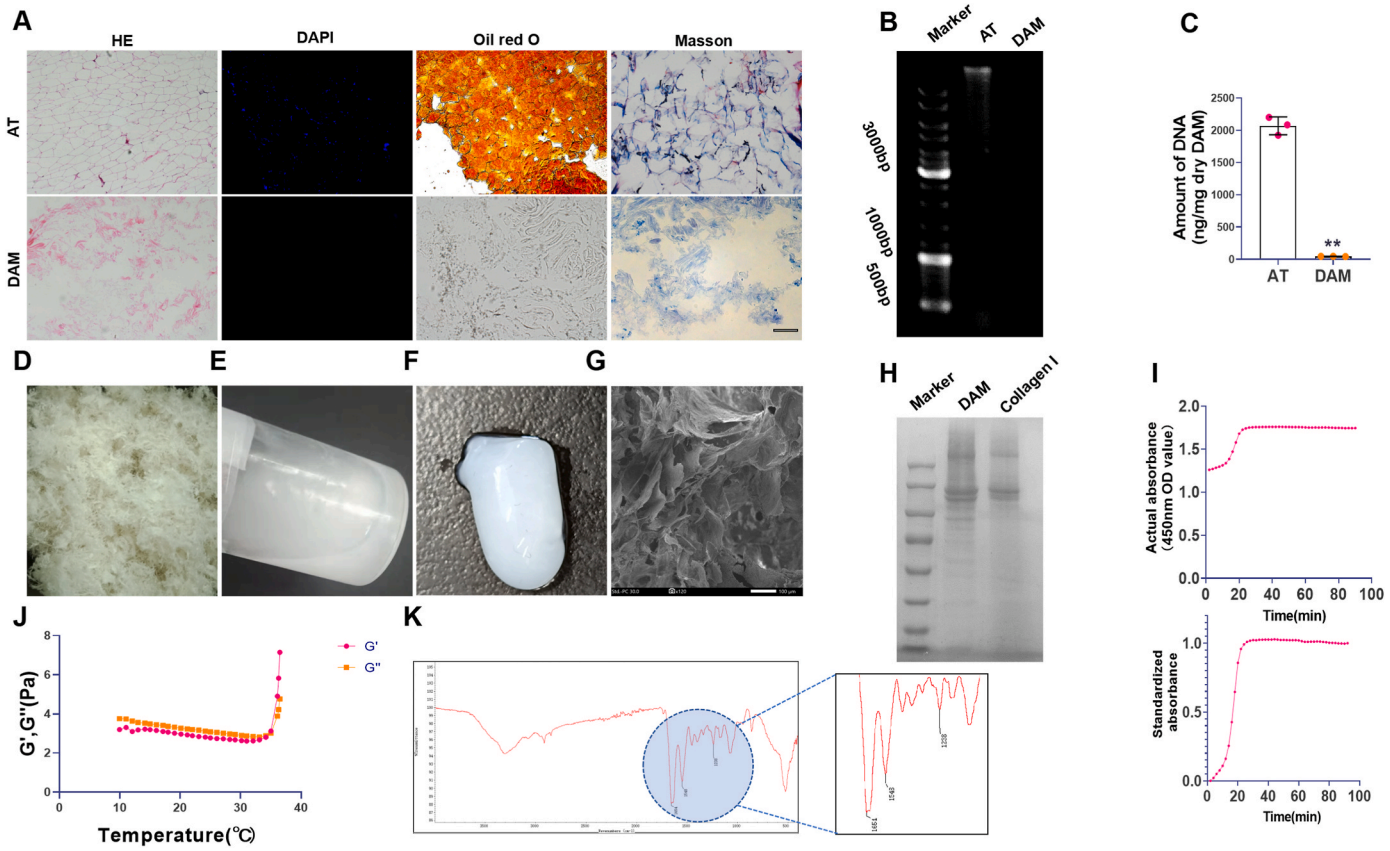

Fig. 2. Characterization of the DAM hydrogel. (A). Representative HE staining, DAPI staining, oil red O staining, and Masson staining images of AT and DAM, scale bar, 100 μm. **(B).** DNA agarose gel electrophoresis. **(C).** The residual DNA quantification in AT and DAM , $^{**}p < 0.01$ *Vs.* AT; n = 3. **(D).** DAM power. **(E).** DAM hydrogel. **(F).** The gel effect of DAM hydrogel in vitro. **(G).** Scanning electron micrograph of DAM hydrogel, scale bar, 100 μm. **(H).** The protein composition analysis of DAM hydrogel and collagen I hydrogel. **(I)**Turbidimetric gelation kinetic of DAM hydrogel. **(J).** The curves of DAM hydrogel in the storage modulus (G′) and the loss modulus(G″) after inducing gelation. **(K).** FTIR spectra of DAM hydrogel. (For interpretation of the references to color in this figure legend, the reader is referred to the Web version of this article.)

3. Results

3.1. MiR-150-5p was upregulated while Notch3 was downregulated in AAA

To determine whether miR-150-5p and Notch3 were involved in AAA development, we detected miR-150-5p and Notch3 expression in rat AAA models. After treatment of $Cacl_2$ for 4 weeks or elastase for 2 weeks, aortic tissues were collected. The qRT-PCR analysis showed that the expression of miR-150-5p was substantially higher in AAA than that in normal aortas in these two models. However, the expression of Notch3 was substantially lower in AAAs compared with that in normal aortas (Fig. 1A and B). Immunohistochemistry results showed that Notch3 was predominantly deposited in the media layer of the aorta, and was significantly lower in both kinds of AAAs *Vs.* Sham aortas (Fig. 1C and D). The upregulated miR-150-5p and downregulated Notch3 in AAA models suggested that they may play important roles in AAA progression.

3.2. Characterization of the DAM hydrogel

Using our previous optimized decellularization protocol, the cellular components and lipids were completely removed from the adipose (Fig. 2A and 3). The amount of DNA in the DAM matrix (48 ± 53.01 ng/mg) is significantly lower than that in adipose tissue (2000 ± 53.01 ng/mg) (Fig. 2B and C). Masson's staining showed that DAM still retained many collagenous structures (Fig. 2A). Then the DAM was lyophilized, powdered (Fig. 2D) and digested for the preparation of DAM hydrogel (Fig. 2E). After 37°C 30 min, flowable DAM hydrogel transformed into non-liquid gel (Fig. 2F). Scanning electron microscopy showed DAM hydrogel possessed abundant pores and fibrillar structure (Fig. 2G). SDS-PAGE analysis showed that there were more peptides and small molecular weight peptide fragments in DAM compared with the macromolecular peptide in collagen I (Fig. 2H).

The gelation kinetics of DAM hydrogel was evaluated, and the turbidimetric gelation kinetics curves of DAM hydrogel showed S-shape (Fig. 2I). Additionally, the rheological characteristic of DAM hydrogel was determined using a parallel plate rheometer. When the temperature was increased to 35°C, solid like behavior of DAM hydrogel was determined for the storage (G′) was greater than the loss modulus (G″) (Fig. 2J). FTIR spectra demonstrated the presence of peaks in DAM associated with collagen (amide I (1654 cm-1), amide II (1548 cm-1) and amide III (1238 cm-1)) (Fig. 2K).

3.3. The swelling, degradation, and cytocompatibility of DAM hydrogel

The wet DAM hydrogel swelled 6.1% in 24 h and remained morphologically intact (Fig. 3A). Additionally, the compressive strength of DAM hydrogel was 36.03 ± 6.2 kPa, and the compressive strength of arterial peripheral adipose tissue was 84 ± 20.26 kPa (Fig. 3B). In vitro degradation of DAM hydrogel was monitored as a function of weight loss over time in collagenase and PBS solution at 37°C. It is clearly observed that the weight loss of hydrogel samples gradually increased over time. About 69% DAM hydrogel could be retained at 7th day in PBS, only 5% DAM hydrogel could be retained at 7th day in collagenase solution (Fig. 3C).

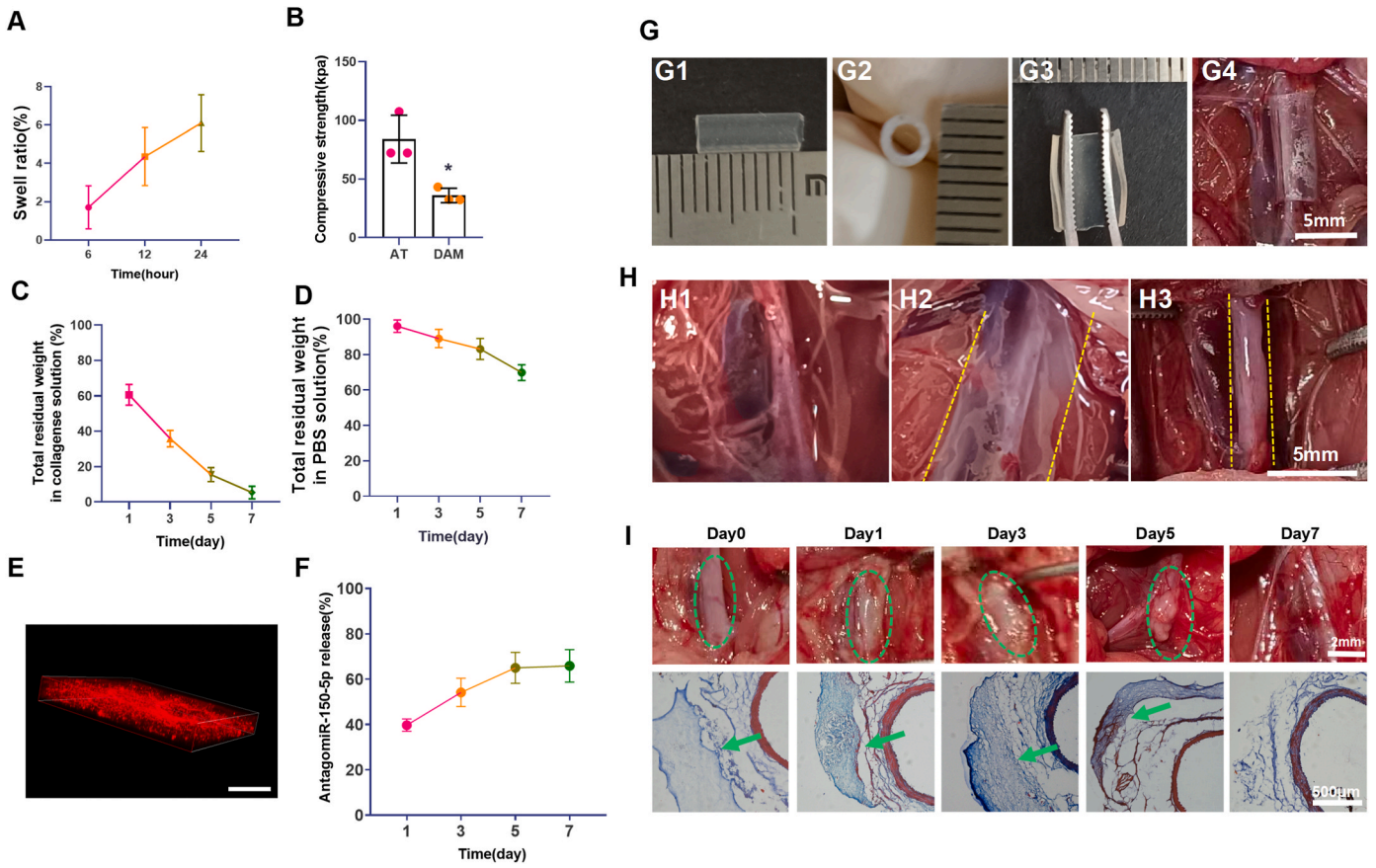

Fig. 3. The swelling, degradation, and delivery of DAM hydrogel (A). The swelling test of DAM hydrogel. **(B).** The compressive test of DAM hydrogel and aortic peripheral adipose tissue, *p < 0.05 *Vs*. AT. AT: aortic peripheral adipose tissue. **(C).** The degradation of DAM hydrogel in collagenase solution. **(D).** The degradation of DAM hydrogel in PBS. **(E).** The distribution of antagomiR-150-5p in DAM hydrogel, scale bar, 100 μm. **(F).** The release of antagomiR-150-5p in DAM hydrogel, n = 3. AT: adipose tissue, DAM: decellularized adipose matrix. **(G).** The length (G1), inner diameter (G2), and the incision (G3) of the silicone hose mold. The silicone hose mold wrapping the abdominal aorta. **(H).** Images of abdominal aorta (H1). Images of DAM hydrogel delivery on the surface of abdominal aorta (H2) or with silicone hose mold around the abdominal aorta (H3). The yellow dotted lines showed the gel location. **(I).** The degradation of DAM hydrogel. The distribution of DAM hydrogel is shown at 0, 1, 3, 5, 7 days in the upper panel, the green circle indicated the DAM hydrogel. In the lower panel, Masson's staining showed the DAM hydrogel (Green arrow) around the abdominal aorta at 0, 1, 3, 5, 7 days. (For interpretation of the references to color in this figure legend, the reader is referred to the Web version of this article.)

To evaluate the toxicity of DAM hydrogel, VSMCs, HUVECs and L929 fibroblasts were treated with the leach liquor of DAM hydrogel for 7 days. We found that no significant cytotoxicity was observed in these cells (Fig. 3D, Fig. S1). The cell viability values were higher than 90%, which was much higher than the cytotoxicity limit (70%) [26]. Taken together, the results showed that DAM hydrogel was an ideal carrier for safe implantation.

3.4. Antagomir150-5p distribution, release, and uptake

Next, the hydrogel delivery system was constructed to release antagomiR-150-5p in AAA. To visualize antagomiR-150-5p distribution and release in DAM hydrogel, it was labeled with Cy5. The 3D reconstructed confocal laser scanning microscopy image clearly showed uniformly distributed red fluorescent dots (antagomiR-150-5p) inside the hydrogel (Fig. 3E). 65.9% antagomir150-5p in DAM hydrogel was released in 7 days (Fig. 3F), which suggested that most antagomiR-150-5p could be released in one week. The above result confirmed the consistency between the degradation of the hydrogel and the antagomiR-150-5p release profile.

We then evaluate the uptake of antagomiR-150-5p by HUVECs, VSMCs, and fibroblasts. The Cy5 labeled antagomiR-150-5p was incubated with the above cells. The results showed that antagomiR-150-5p could be taken by the cells in a time-dependent manner (Fig. S2).

In further, to evaluate the uptake of the antagomiR-150-5p at the site of AAA, the Cy5 labeled antagomiR-150-5p was delivered via DAM. At 6 h, few red antagomiR-150-5p could be detected in the aorta. However, at 12 h and 24 h, many positive red dots were observed in the aorta. As expected, no positive red staining was observed in the aorta that didn't undergo antagomiR delivery (Fig. S3). This result confirmed that the antagomiR-150-5p could be released to the aorta via DAM.

3.5. Shaping hydrogel around the abdominal aorta by the mold

Usually, the DAM hydrogel was directly delivered to the surface of the abdominal aorta. With this delivery strategy, it is difficult to limit the DAM hydrogel around the aorta. The DAM hydrogel would flow and cover the other tissues besides the abdominal aorta (Fig. 3H2, Video 3). To solve this problem, a silicone hose of 2 mm internal diameter (length in 8 mm) with an incision along the longitudinal axis was used as the mold for shaping and immobilizing DAM hydrogel around the abdominal aorta (Fig. 3G). After injection the DAM hydrogel into the space between the abdominal aorta and silicone hose, a white gel was formed around the abdominal aorta in 30 min at 37°C(Fig. 3H3). In further, in vivo the DAM hydrogel could be observed at the periphery of aorta till the 7th day through the general observation and the corresponding sections with Masson's staining (Fig. 3I). The above results indicated that the DAM hydrogel could accurately located around the aorta.

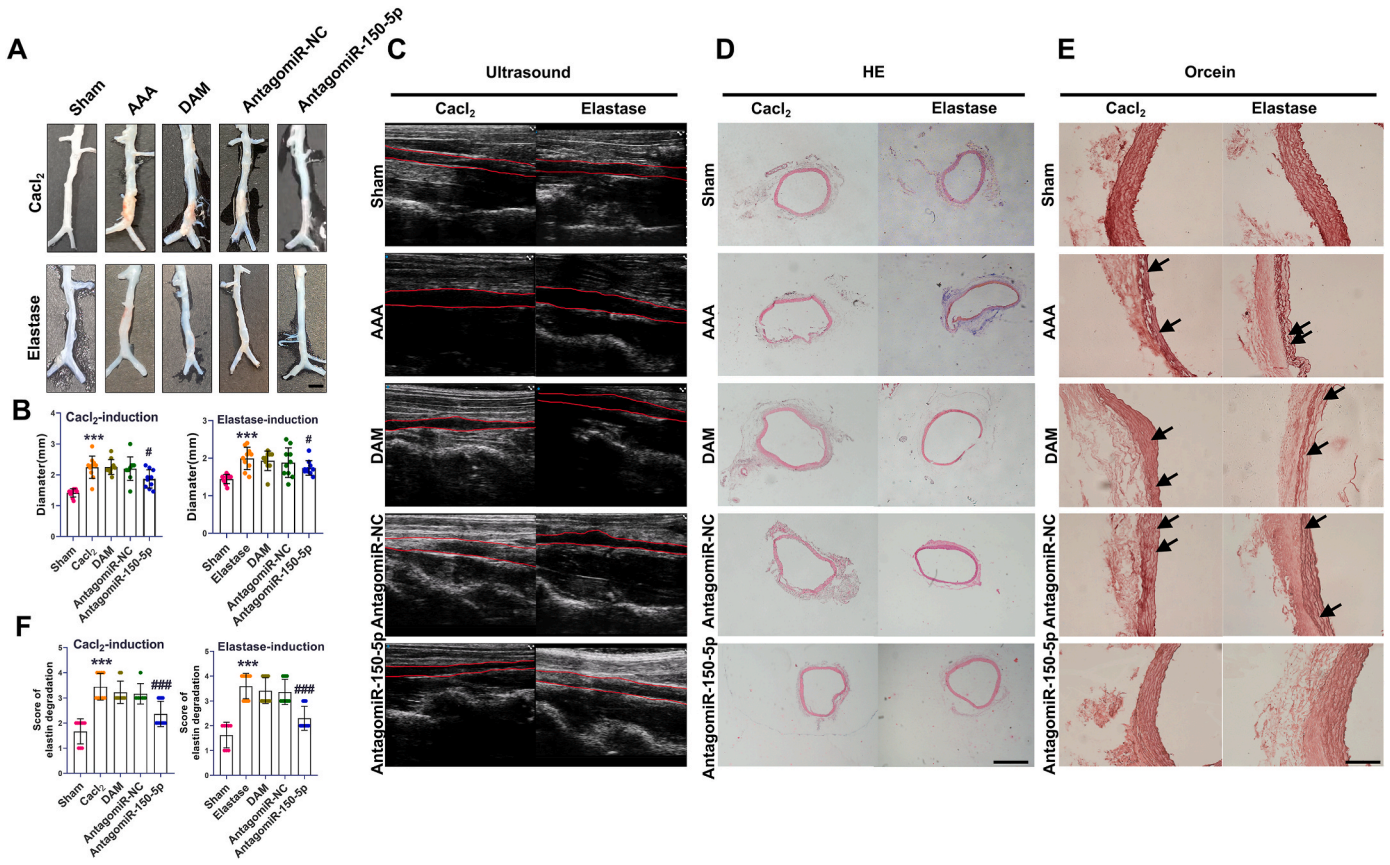

Fig. 4. AntagomiR-150-5p delivery attenuated the aortic wall expansion in rat AAA. (A). Representative images showing the diameters of the aortas in $Cacl_2$-induced AAA and elastase-induced AAA, scale bar, 3 mm. **(B).** Diameters of the aortas analysis in $Cacl_2$-induced AAA and elastase-induced AAA. ***P < 0.001, *Vs.* sham group, #P < 0.05 *Vs.* AAA group. **(C).** Representative two-dimensional ultrasound images of aortas in $Cacl_2$-induced AAA and elastase-induced AAA. **(D).** Representative HE images of aortas in $Cacl_2$-induced AAA and elastase-induced AAA, scale bar, 200 μm. **(E).** Images of Orcein staining in AAA models, scale bar, 200 μm. **(F).** Analysis of Orcein staining in AAA models, n = 6-10, ***P < 0.001, *Vs.* sham group; $^{\#\#\#}$P < 0.001 *Vs.* AAA group.

3.6. AntagomiR-150-5p delivery attenuated the aortic wall expansion in rat AAA

Aortic dilation or rupture is the major feature of AAA. In $Cacl_2$ induced AAA, the aortic diameter was significantly increased in the AAA group compared to the normal group. However, antagomiR-150-5p treatment significantly prevented the AAA development. Similarly, in elastase-induced AAA, antagomiR-150-5p treatment also attenuated the aortic dilation in AAA (Fig. 4A–D). The results concluded that miR-150-5p inhibition effectively repressed the aortic wall expansion in rat AAA.

3.7. Antagomir150-5p delivery ameliorated elastin fragmentation and VSMCs depletion in rat AAA

Degradation of aortic elastin is a prominent feature of abdominal aortic aneurysm. Orcein staining showed that the elastic lamellae became flat, and the elastin fragmentation (black arrow) emerged in AAA group whereas antagomiR-150-5p treatment obviously reduced degradation of elastin (Fig. 4E and F).

In addition, the depletion of VSMCs is a crucial factor during AAA formation. α-SMA, as the biomarker of VSMCs, was detected in this study by immunohistochemical staining. Our results showed that α-SMA expression in AAA groups was decreased significantly compared with normal groups, however, the decreased α-SMA expression could be relieved by delivery of antagomiR-150-5p (Fig. S4).

3.8. AntagomiR-150-5p delivery attenuated the inflammation in rat AAA

To evaluate the preventive effect of antagomiR-150-5p on inflammation in AAA, immunohistochemical detection of CD45, CD68, MCP-1, and TNF-α in the aorta were performed. The result showed that the number of CD45 positive cells and CD68 positive cells in the aorta of the AAA group were increased compared with the normal group, indicating an increase in infiltration of leukocytes and macrophages in both AAA models. However, with antagomiR-150-5p treatment, the infiltration of inflammatory cells in the aorta of AAA was significantly suppressed. Moreover, the expression of MCP-1 and TNF-α were increased in AAA, which were also significantly inhibited by antagomiR-150-5p delivery (Fig. 5). These results suggested that the inhibition of miR-150-5p could attenuate inflammation during AAA formation.

3.9. AntagomiR-150-5p delivery abolished the upregulation of NF-κB (p65), MMP-2, and MMP-9, and reversed the downregulation of Notch3 expression in rat AAA

NF-κB activation plays a key role in the inflammatory process. MMP-2 and MMP-9 are closely related to ECM degradation in the pathogenesis of AAA. Our results showed that NF-κB(p65), MMP-2, and MMP-9 in the AAA group were increased compared with the normal group, which was decreased after antagomiR-150-5p delivery. Additionally, the decreased Notch3 in two rat AAA models was increased after antagomiR-150-5p delivery. Meanwhile, antagomiR-150-5p upregulated the down-regulation of elastin in the aortas of the AAA (Fig. 6). This result was consistent with the Ocerin staining changes.

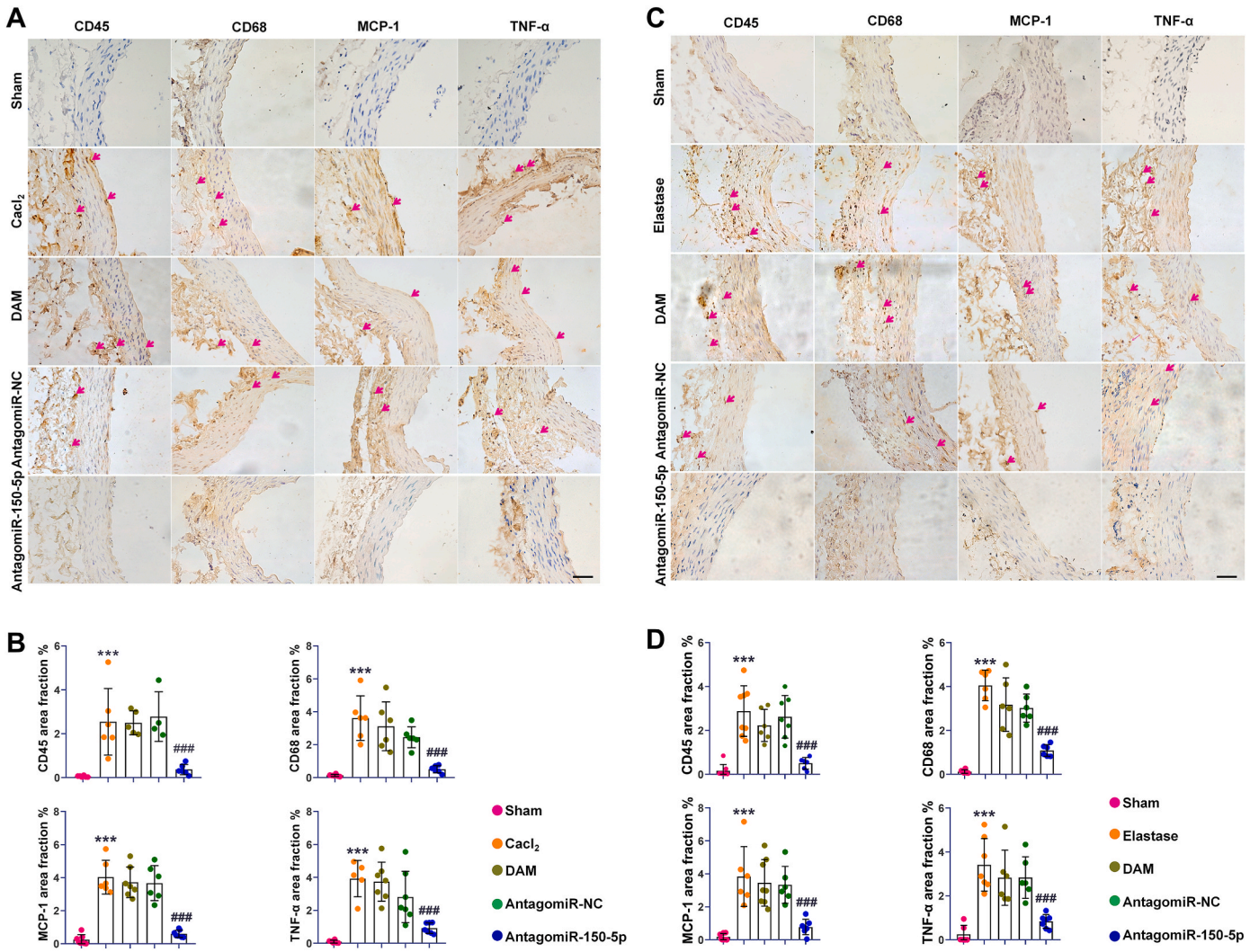

Fig. 5. AntagomiR-150-5p delivery attenuated the inflammation in rat AAA. (A, B). Representative photomicrographs and semiquantitative analysis of CD45, CD68, MCP-1 and TNF-α of immunostaining in $Cacl_2$-induced AAA, scale bars, 50 μm, n = 6, ***P < 0.001 *Vs.* sham group; $^{###}$P < 0.001 *Vs.* AAA group. **(C, D).** Representative photomicrographs and semiquantitative analysis of CD45, CD68, MCP-1 and TNF-α of immunostaining in elastase-induced AAA, scale bars, 50 μm, n = 6, ***P < 0.001 *Vs.* sham group; $^{###}$P < 0.001 *Vs.* AAA group.

3.10. MiR-150-5p inhibition downregulated NF-κB(p65), MMP-2, MMP-9, and upregulated elastin in VSMCs

To further explore the mechanism of miR-150-5p in the development of AAA, VSMCs were treated with TNF-α as the AAA model in vitro. Like the previous observation in rat AAA, we found that miR-150-5p was increased, and Notch3 was decreased in VSMCs after TNF-α treatment (Fig. S5).

Then we explored whether there are functional correlations among miR-150-5p, NF-κB (p65), MMP-2, MMP-9, and elastin. MiR-150-5p inhibitor and miR-150-5p mimics were transfected into VSMCs for 48 h respectively, followed by TNF-α treatment. Western blot results showed that the expression of NF-κB (p65), MMP-2, and MMP-9 were increased and the levels of elastin and Notch3 were decreased in VSMCs with TNF-α stimulation. However, these effects were abolished with miR-150-5p inhibition, while exacerbated with miR-150-5p overexpression (Fig. 7). These results suggested that miR-150-5p may participate in AAA formation via regulating the expression of NF-κB (p65), MMP-2, MMP-9, and elastin in VSMCs.

3.11. MiR-150-5p regulated the expression of MMP-2, MMP-9, NF-κB (p65) and elastin via Notch3 in VSMCs

To evaluate whether miR-150-5p/Notch3 was involved in regulating MMP-2, MMP-9, NF-κB (p65) and elastin, the miR-150-5p inhibitor and Notch3 lentiviral-mediated stable knockdown were co-transfected to VSMCs, following with TNF-α treatment. These results demonstrated that the expression of Notch3 and elastin were downregulated with TNF-α treatment and downregulated further with Notch3 knockdown but regulated back after miR-150-5p inhibition. Inversely, the levels of MMP-2, MMP-9, and NF-κB (p65) were upregulated with TNF-α treatment and upregulated further with Notch3 knockdown but regulated back after miR-150-5p inhibition. These data suggest that miR-150-5p regulated the expression of MMP-2, MMP-9, NF-κB (p65), and elastin via Notch3 in VSMCs (Fig. 8).

4. Discussion

AAA is an asymptomatic degenerative disease, arises from pathological changes in the aortic wall, including the loss of VSMCs and degradation of the ECM. Currently, open surgery and endovascular repair are the main measures to repair AAA [27]. It is essential to explore

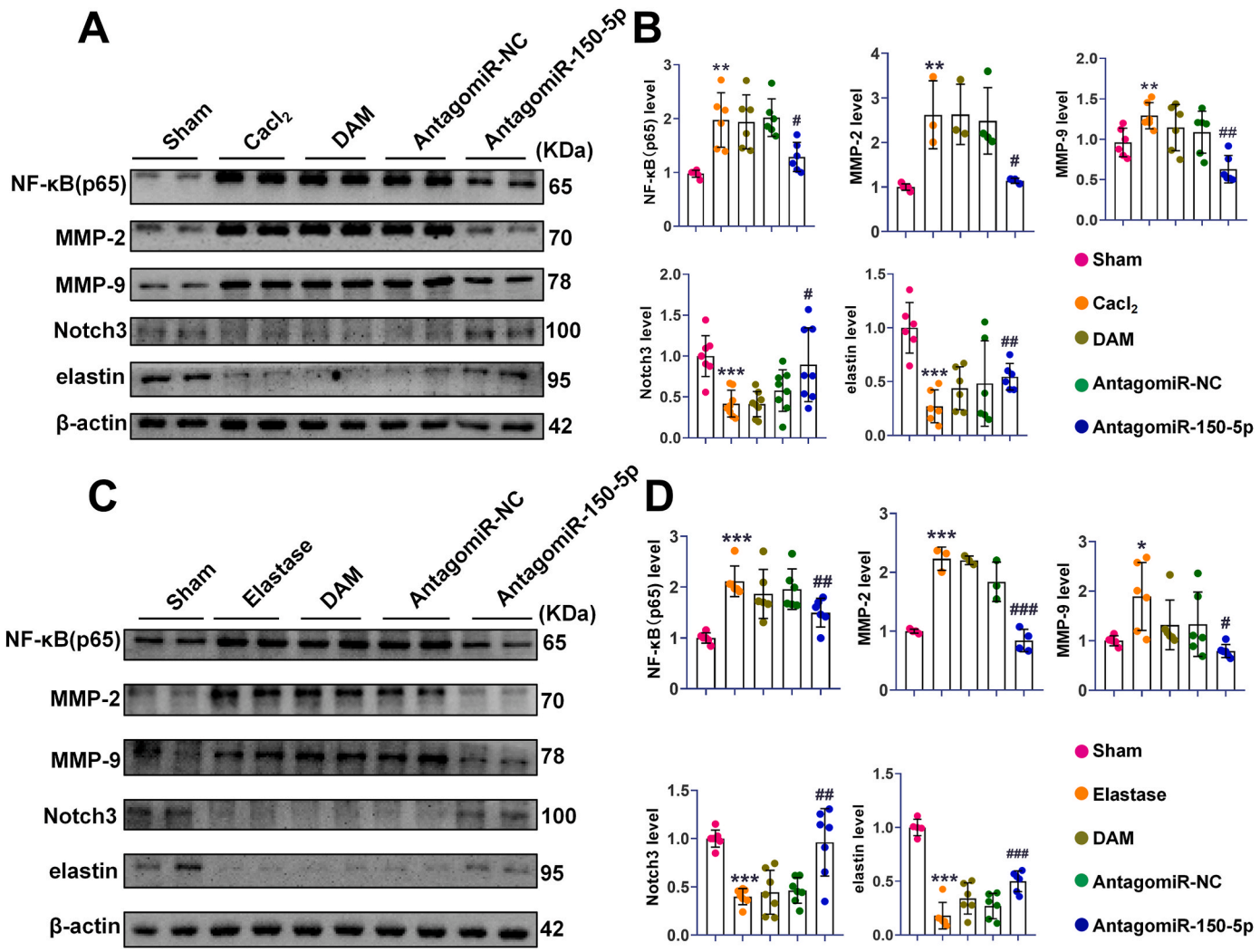

Fig. 6. AntagomiR-150-5p delivery abolished the upregulation of NF-κB (p65), MMP-2, and MMP-9, and reversed the downregulation of Notch3 and elastin expression in the aortas of AAA rats. (A). Representative Western blot bands and analysis of NF-κB (p65), MMP-2, MMP-9, Notch3 and elastin in $Cacl_2$-induced AAA model. (B). Quantitative analysis of NF-κB (p65), MMP-2, MMP-9, Notch3 and elastin in $Cacl_2$-induced AAA model, $^{*}P < 0.05$, $^{**}P < 0.01$, $^{***}P < 0.001$ *Vs.* sham group; $^{\#}P < 0.05$, $^{\#\#}P < 0.01$ *Vs.* AAA group. (C). Representative Western blot bands of NF-κB (p65), MMP-2, MMP-9, Notch3 and elastin in elastase-induced AAA model. (D). Quantitative analysis of NF-κB (p65), MMP-2, MMP-9, Notch3 and elastin in elastase-induced AAA model, $^{*}P < 0.05$, $^{**}P < 0.01$, $^{***}P < 0.001$ *Vs.* sham group; $^{\#}P < 0.05$, $^{\#\#}P < 0.01$, $^{\#\#\#}P < 0.001$ *Vs.* AAA group.

new effective approaches on the prevention of AAA development. In this study, we demonstrated for the first time that delivery of antagomiR-150-5p by DAM hydrogel could prevent the development of $Cacl_2$-induced AAA and elastase-induced AAA. To be specific, aortic dilation and elastin degradation were inhibited with antagomiR-150-5p treatment. Moreover, antagomiR-150-5p delivery suppressed inflammatory cell infiltration and the expression of inflammatory cytokines and rescued the downregulated Notch3 and α-SMA in rat AAA. The beneficial effect of antagomiR-150-5p on the development of AAA may be achieved through regulating Notch3.

MicroRNAs are involved in cardiovascular diseases, such as heart failure, neointima formation and atherosclerosis [28,29]. It was reported that microRNAs also play crucial roles in the development of AAA [30–32]. Recent study showed that there was an abnormal miR-150-5p expression level in the plasma of patients with sub-aneurysmal aortic dilation, which suggests miR-150-5p may participate in the pathogenesis of AAA [33]. In this study, we showed that the level of miR-150-5p was significantly upregulated in two kinds of rat AAA models.

AntagomiR treatment is one of the effective approaches in RNA-targeted therapeutics [34,35]. In our study, antagomiR-150-5p was used to suppress miR-150-5p function in rat AAA. After antagomiR-150-5p delivery, the expansion of aortic wall in rat AAA models was eased. AAA dilation and rupture were tightly associated with the breakdown of elastin within the aorta [36]. Histological staining results showed that the elastic lamellae in the AAA group became straight, and more fragmentation were observed than normal tissue, which could be attenuated with antagomiR-150-5p delivery. Moreover, antagomiR-150-5p could rescue the downregulation of elastin in the aortas of rat AAA. Depletion of VSMCs is another important feature during AAA formation. Our results showed that antagomiR-150-5p attenuated the decreased α-SMA in AAA development.

To evaluate the direct role of miR-150-5p inhibition in AAA development, the effective delivery of the antagomiR-150-5p to the aorta tissue is the key step to be considered. Perivascular administration is a promising approach in treating the focal vascular pathologies, such as coronary interventions, arteriovenous fistulas placements and carotid surgery etc [37]. Recent studies demonstrated that perivascular application of drugs could effectively decrease AAA development and intimal hyperplasia through different drug delivery system [13,38]. Currently, in clinics there are no approved strategies on targeted local perivascular prevention. Therefore, perivascular administration for treating AAAs

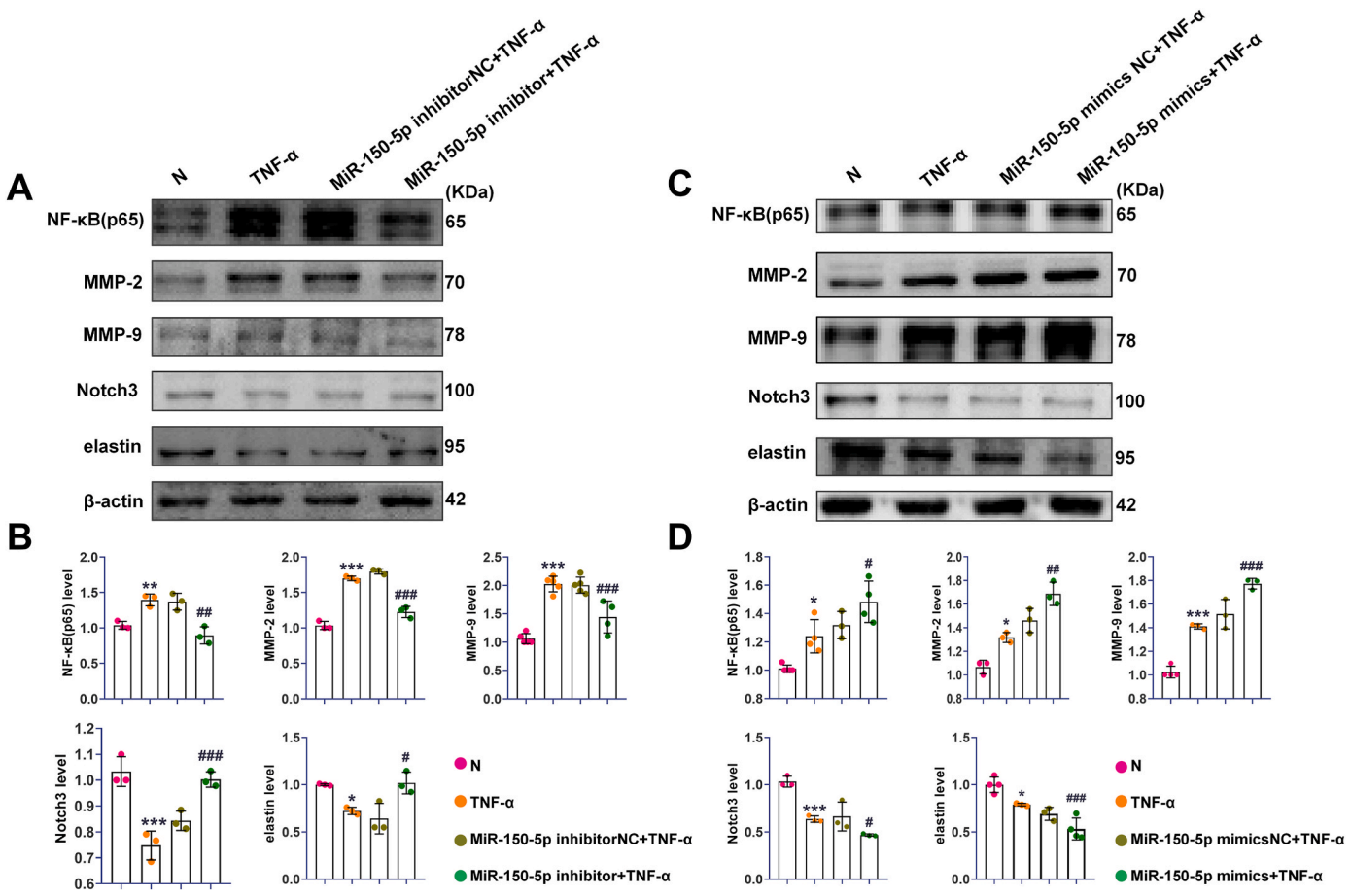

Fig. 7. MiR-150-5p regulated the expression of NF-κB (p65), MMP-2, MMP-9, Notch3 and elastin in VSMCs with TNF-α treatment. (A). Representative Western blot bands of NF-κB (p65), MMP-2, MMP-9, Notch3 and elastin in VSMCs with miR-150-5p inhibition and TNF-α treatment. (B). Quantitative analysis of NF-κB (p65), MMP-2, MMP-9, Notch3 and elastin in VSMCs with miR-150-5p inhibition and TNF-α treatment, *P < 0.05, **P < 0.01, ***P < 0.001 *Vs.* N group; $^{\#}$P < 0.05, $^{\#\#}$P < 0.01, $^{\#\#\#}$P < 0.001 *Vs.* TNF-α group. (C). Representative Western blot bands of NF-κB(p65), MMP-2, MMP-9, Notch3 and elastin in VSMCs with miR-150-5p overexpression and TNF-α treatment. (D). Quantitative analysis of NF-κB(p65), MMP-2, MMP-9, Notch3 and elastin in VSMCs with miR-150-5p overexpression and TNF-α treatment, *P < 0.05, **P < 0.01, ***P < 0.001 Vs. N group; $^{\#}$P < 0.05, $^{\#\#}$P < 0.01, $^{\#\#\#}$P < 0.001 *Vs.* TNF-α group.

may help future translational advances. To efficiently release drugs or compounds, a biodegradable delivery system should be applied around the vessel for an extended time. In recent years, hydrogels have been widely applied in various fields including flexible sensors, wearable devices, soft robots, regenerative medicine, and so on [39]. Especially, the extracellular matrix hydrogels have the similarity to some bio-architectures, which was endowed with bio-mimetic and bio-functional properties [40]. The adipose tissue around the abdominal aorta plays important roles in vascular homeostasis [18]. DAM is derived from adipose tissue, which has the similar components and structure to adipose tissue. In further, DAM hydrogel could be a release platform to secrete paracrine factors [41]. To provide a similar micro-environment in situ in the aorta, DAM hydrogel-based delivery system was developed in this study. The direct application of hydrogel on the aorta will lead to an uneven distribution or flowing to other tissues besides the aorta. We designed a silicone tube mold around the abdominal aorta for distributing the DAM hydrogel precisely and evenly to the arterial periphery. DAM hydrogel could be self-assembled to form gel around the aorta with no cytotoxicity on ECs, VSMCs, and fibroblasts (Fig. S1), and sustain release antagomiR-150-5p (Fig. 3F).

The Inflammatory response is one of the main characteristic features of AAA. Inflammation increases MMP levels, which induces ECM destruction and aortic wall remodeling in AAA [2]. In this study, we found that there existed many leucocytes and macrophages in the arterial wall in rats AAA. However, antagomiR-150-5p treatment attenuated the inflammation as evidenced by reducing inflammatory cells infiltration in AAA. Meanwhile, inflammatory activation was detected as evidenced by significant upregulation of MCP-1, TNF-α and NF-κB (p65) in aortic wall in AAA. NF-κB (p65) is known to be involved in AAA pathogenesis [20]. Specifically, the inflammatory activation was effectively suppressed with antagomiR-150-5p delivery as evidenced by obviously decreased the above inflammatory cytokines. MMP-2 and MMP-9 were detected after antagomiR-150-5p delivery as well. We found that antagomir150-5p could abolish the upregulation of NF-κB (p65), MMP-2, and MMP-9 in rat AAA. Recent study also demonstrated that miR-150 deletion could reduce NF-κBrelated inflammation in cardiac fibroblasts [42].

To further verify the effect of miR-150-5p inhibition on the AAA formation, VSMCs were treated with TNF-α to mimic the inflammation micro-environment in AAA. After TNF-α treatment, miR-150-5p level was increased and Notch3 was decreased in VSMCs. This result was accorded with rat AAA as well. Decreased activation of NF-κB(p65), MMP-2, and MMP-9 and increased elastin level was detected after miR-150-5p inhibition. In contrast, over-expression of miR-150-5p could upregulate NF-κB (p65), MMP-2, and MMP-9 and downregulate elastin level. These data validated the results of animal experiments with the delivery of antagomiR-150-5p.

Notch proteins are widely expressed in many species. Mammals have four Notch receptors (Notch1-4) and five transmembrane ligands (Jagged1, Jagged2, Delta-like1, Delta-like3, and Deltalike4) [43]. Notch3

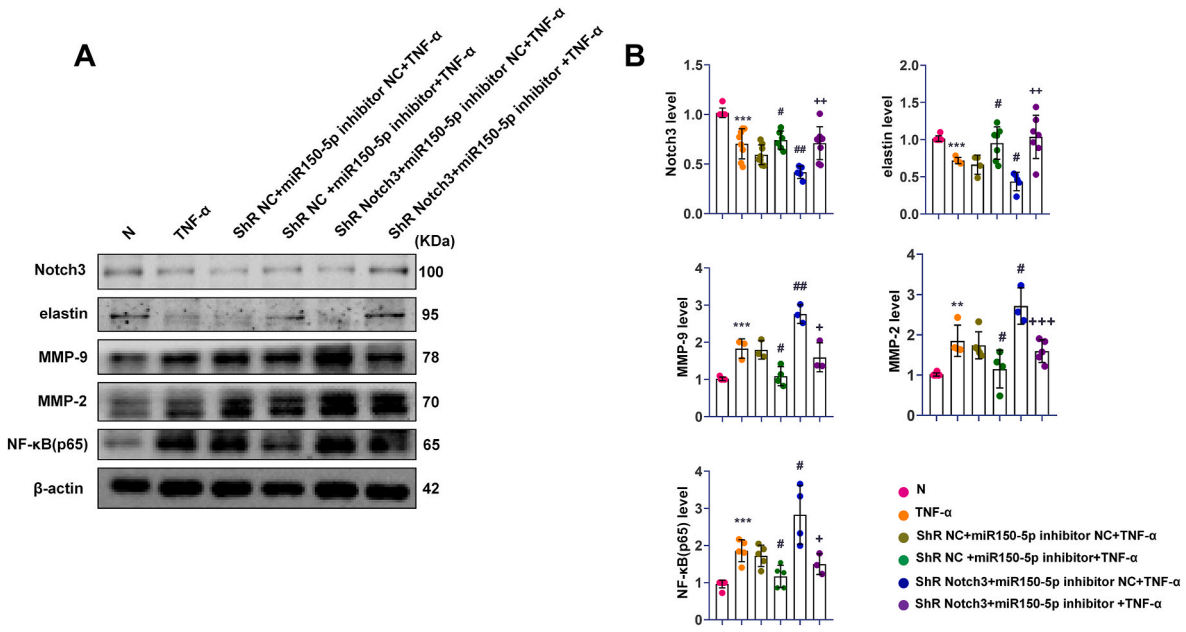

Fig. 8. MiR-150-5p regulated the expression of MMP-2, MMP-9, NF-κB (p65) and elastin via Notch3 in VSMCs with TNF-α treatment. (A). Representative Western blot bands of NF-κB (p65), MMP-2, MMP-9, Notch3 and elastin in shR-VSMCs with miR-150-5p inhibition and TNF-α treatment. (B). Quantitative analysis of NF-κB(p65), MMP-2, MMP-9, Notch3 and elastin in shR-VSMCs with miR-150-5p inhibition and TNF-α treatment. ***P < 0.001 *Vs.* N group; $^{\#}$P < 0.05, $^{\#\#}$P < 0.01 *Vs.* shR NC + miR-150inhibitor NC + TNF-α group; $^{+}$P<0.05, $^{++}$P<0.01 *Vs.* shR Notch3 + miR-150inhibitor NC + TNF-α group; N, normal VSMCs; shR NC, VSMCs transfected GFP lentiviral vector; shR Notch3, VSMCs transfected shR-Notch3 lentiviral vector.

could regulate vascular development and physiology via VSMCs [44]. In the Notch3-deficient mice, the diameters of arteries were enlarged, smooth muscle layers became thinner and disorganized, and the number of elastic laminae was decreased [45]. Previous study reported that Notch3 was significantly downregulated in human AAAs [46]. Our study demonstrated that Notch3 was decreased in two types of rat AAA as well. Our previous study revealed that Notch3 could be targeted by miR-150-5p in adipogenesis [41]. A recent study showed that Notch3 knockout mice failed to activate proinflammatory cytokines [47]. However, whether Notch3 is correlated with the above cytokines in AAA formation is largely unknown. We found that in VSMCs with Notch3 knockdown stimulated by TNF-α, the expression of Notch3 and elastin were further downregulated compared with control group but regulated back after miR-150-5p inhibition. Inversely, the level of MMP-2, MMP-9, and NF-κB (p65) were increased than control group but regulated back after miR-150-5p were inhibited. In hepatocellular carcinoma, Notch3 could reduce the invasion capacity by regulating MMP-2 and MMP-9 [46]. These results indicated that miR-150-5p could target Notch3 thereby regulating the expression of MMP-2, MMP-9, NF-κB (p65), and elastin to participate in AAA formation.

5. Conclusion

In summary, we provide an effective way for preventing AAA via DAM hydrogel immobilized on the adventitia to release antagomiR-150-5p in rats. Our work demonstrated that the inhibition of miR-150-5p could prevent AAA formation by inhibiting inflammation and MMPs and facilitating the biosynthesis of elastin. This beneficial effect may be achieved by regulation Notch3.

CRediT authorship contribution statement

Xin Chen: Writing – original draft, Methodology, Investigation. **Shoushuai Wang:** Methodology, Investigation. **Weijian Hou:** Methodology, Investigation. **Yanhui Zhang:** Methodology. **Yapeng Hou:** Methodology. **Hao Tong:** Formal analysis. **Xiaoxin Zhang:** Validation, Investigation. **Yue Liu:** Investigation. **Ruoxuan Yang:** Software. **Xiang Li:** Writing – review & editing, Methodology. **Qin Fang:** Writing – review & editing, Methodology. **Jun Fan:** Writing – review & editing, Supervision, Funding acquisition, Conceptualization.

Declaration of competing interest

The authors declare that they have no known competing financial interests or personal relationships that could have appeared to influence the work reported in this manuscript.

Acknowledgments

This work was supported by Liaoning Provincial Central Guide local science and technology development fund plan, China [no. 2024JH6/100800021], Liaoning Revitalization Talents Program, China [no. XLYC1907124] and the Scientific Research Fund of Educational Department of Liaoning Province of China [No. LJKMZ20221203].

Appendix A. Supplementary data

Supplementary data to this article can be found online at https://doi.org/10.1016/j.mtbio.2024.101350.

Data availability

Data will be made available on request.

References

[1] G. Ailawadi, J.L. Eliason, G.R. Upchurch, Current concepts in the pathogenesis of abdominal aortic aneurysm, J. Vasc. Surg. 38 (3) (2003) 584–588.
[2] H. Li, H. Xu, H. Wen, H. Wang, R. Zhao, Y. Sun, C. Bai, J. Ping, L. Song, M. Luo, J. Chen, Lysyl hydroxylase 1 (LH1) deficiency promotes angiotensin II (Ang II)-induced dissecting abdominal aortic aneurysm, Theranostics 11 (19) (2021) 9587–9604.
[3] J. Golledge, Abdominal aortic aneurysm: update on pathogenesis and medical treatments, Nat. Rev. Cardiol. 16 (4) (2019) 225–242.

[4] B.W. Ullery, R.L. Hallett, D. Fleischmann, Epidemiology and contemporary management of abdominal aortic aneurysms, Abdom Radiol (NY) 43 (5) (2018) 1032–1043.
[5] T.X. Lu, M.E. Rothenberg, MicroRNA, J. Allergy Clin. Immunol. 141 (4) (2018) 1202–1207.
[6] F.-H. Gong, W.-L. Cheng, H. Wang, M. Gao, J.-J. Qin, Y. Zhang, X. Li, X. Zhu, H. Xia, Z.-G. She, Reduced atherosclerosis lesion size, inflammatory response in miR-150 knockout mice via macrophage effects, J. Lipid Res. 59 (4) (2018) 658–669.
[7] J. Fan, S. Wang, X. Lu, Z. Sun, Transplantation of bone marrow cells from miR150 knockout mice improves senescence-associated humoral immune dysfunction and arterial stiffness, Metabolism 134 (2022) 155249.
[8] H.E. Morris, K.B. Neves, A.C. Montezano, M.R. MacLean, R.M. Touyz, Notch3 signalling and vascular remodelling in pulmonary arterial hypertension, Clin. Sci. (Lond.) 133 (24) (2019) 2481–2498.
[9] J.J. Hofmann, M.L. Iruela-Arispe, Notch signaling in blood vessels: who is talking to whom about what? Circ. Res. 100 (11) (2007) 1556–1568.
[10] Y.-K. Tao, H. Zeng, G.-Q. Zhang, S.T. Chen, X.-J. Xie, X. He, S. Wang, H. Wen, J.-X. Chen, Notch3 deficiency impairs coronary microvascular maturation and reduces cardiac recovery after myocardial ischemia, Int. J. Cardiol. 236 (2017) 413–422.
[11] E. Biros, P.J. Walker, M. Nataatmadja, M. West, J. Golledge, Downregulation of transforming growth factor, beta receptor 2 and Notch signaling pathway in human abdominal aortic aneurysm, Atherosclerosis 221 (2) (2012) 383–386.
[12] G. Alessandri, V. Coccè, F. Pastorino, R. Paroni, M. Dei Cas, F. Restelli, B. Pollo, L. Gatti, C. Tremolada, A. Berenzi, E. Parati, A.T. Brini, G. Bondiolotti, M. Ponzoni, A. Pessina, Microfragmented human fat tissue is a natural scaffold for drug delivery: potential application in cancer chemotherapy, J. Contr. Release : official journal of the Controlled Release Society 302 (2019) 2–18.
[13] Y. Wei, H. Jiang, F. Li, C. Chai, Y. Xu, M. Xing, W. Deng, H. Wang, Y. Zhu, S. Yang, Y. Yu, W. Wang, Y. Wei, Y. Guo, J. Tian, J. Du, Z. Guo, Y. Wang, Q. Zhao, Extravascular administration of IGF1R antagonists protects against aortic aneurysm in rodent and porcine models, Sci. Transl. Med. 16 (745) (2024) eadh1763.
[14] C.J. Leclerc, T.T. Cooper, G.I. Bell, G.A. Lajoie, L.E. Flynn, D.A. Hess, Decellularized adipose tissue scaffolds guide hematopoietic differentiation and stimulate vascular regeneration in a hindlimb ischemia model, Biomaterials 274 (2021) 120867.
[15] H. Zhou, Z. He, Y. Cao, L. Chu, B. Liang, K. Yu, Z. Deng, An injectable magnesium-loaded hydrogel releases hydrogen to promote osteoporotic bone repair via ROS scavenging and immunomodulation, Theranostics 14 (9) (2024) 3739–3759.
[16] X. Li, S. Liu, S. Han, Q. Sun, J. Yang, Y. Zhang, Y. Jiang, X. Wang, Q. Li, J. Wang, Dynamic stiffening hydrogel with instructive stiffening timing modulates stem cell fate in vitro and enhances bone remodeling in vivo, Adv. Healthcare Mater. 12 (29) (2023) e2300326.
[17] K. Su, J. Li, X. Wu, D. Deng, H. Gu, Y. Sun, X. Wang, W. Huang, Y. Wang, X. Shang, C. Xue, L. Liang, X. Li, D. Li, S. Ang, K. Zhang, P. Wu, K. Wu, One-step synthesis of hydrogel adhesive with acid-responsive tannin release for diabetic oral mucosa defects healing, Adv. Healthcare Mater. 13 (9) (2024) e2303252.
[18] L. Piacentini, J.P. Werba, E. Bono, C. Saccu, E. Tremoli, R. Spirito, G.I. Colombo, Genome-wide expression profiling unveils autoimmune response signatures in the perivascular adipose tissue of abdominal aortic aneurysm, Arterioscler. Thromb. Vasc. Biol. 39 (2) (2019) 237–249.
[19] Y. Zhao, J. Fan, S. Bai, Biocompatibility of injectable hydrogel from decellularized human adipose tissue in vitro and in vivo, J. Biomed. Mater. Res. B Appl. Biomater. 107 (5) (2019) 1684–1694.
[20] T. Xu, S. Wang, X. Li, X. Li, K. Qu, H. Tong, R. Zhang, S. Bai, J. Fan, Lithium chloride represses abdominal aortic aneurysm via regulating GSK3β/SIRT1/NF-κB signaling pathway, Free Radic. Biol. Med. 166 (2021).
[21] A. Lolli, K. Sivasubramaniyan, M.L. Vainieri, J. Oieni, N. Kops, A. Yayon, G.J.V. M. van Osch, Hydrogel-based delivery of antimiR-221 enhances cartilage regeneration by endogenous cells, J. Contr. Release : official journal of the Controlled Release Society 309 (2019) 220–230.
[22] Y. Bi, H. Zhong, K. Xu, X. Qi, Z. Zhang, G. Wu, X. Han, Novel experimental model of enlarging abdominal aortic aneurysm in rabbits, J. Vasc. Surg. 62 (4) (2015) 1054–1063.
[23] F. Wang, X.Q. Zhao, J.N. Liu, Z.H. Wang, X.L. Wang, X.Y. Hou, R. Liu, F. Gao, M. X. Zhang, Y. Zhang, P.L. Bu, Antagonist of microRNA-21 improves balloon injury-induced rat iliac artery remodeling by regulating proliferation and apoptosis of adventitial fibroblasts and myofibroblasts, J. Cell. Biochem. 113 (9) (2012) 2989–3001.
[24] Y.-W. Yan, J. Fan, S.-L. Bai, W.-J. Hou, X. Li, H. Tong, Zinc prevents abdominal aortic aneurysm formation by induction of A20-mediated suppression of NF-κB pathway, PLoS One 11 (2) (2016) e0148536.
[25] M. Yu, C. Chen, Y. Cao, R. Qi, Inhibitory effects of doxycycline on the onset and progression of abdominal aortic aneurysm and its related mechanisms, Eur. J. Pharmacol. 811 (2017) 101–109.
[26] J. Cao, G. He, X. Ning, X. Chen, L. Fan, M. Yang, Y. Yin, W. Cai, Preparation and properties of O-chitosan quaternary ammonium salt/polyvinyl alcohol/graphene oxide dual self-healing hydrogel, Carbohydr. Polym. 287 (2022) 119318.
[27] A.R. Zankl, H. Schumacher, U. Krumsdorf, H.A. Katus, L. Jahn, C.P. Tiefenbacher, Pathology, natural history and treatment of abdominal aortic aneurysms, Clin. Res. Cardiol. 96 (3) (2007) 140–151.
[28] T. Barwari, A. Joshi, M. Mayr, MicroRNAs in cardiovascular disease, J. Am. Coll. Cardiol. 68 (23) (2016) 2577–2584.
[29] F. Fasolo, K. Di Gregoli, L. Maegdefessel, J.L. Johnson, Non-coding RNAs in cardiovascular cell biology and atherosclerosis, Cardiovasc. Res. 115 (12) (2019) 1732–1756.
[30] K. Di Gregoli, N.N. Mohamad Anuar, R. Bianco, S.J. White, A.C. Newby, S. J. George, J.L. Johnson, MicroRNA-181b controls atherosclerosis and aneurysms through regulation of TIMP-3 and elastin, Circ. Res. 120 (1) (2017) 49–65.
[31] L. Maegdefessel, J. Azuma, P.S. Tsao, MicroRNA-29b regulation of abdominal aortic aneurysm development, Trends Cardiovasc. Med. 24 (1) (2014) 1–6.
[32] M.C. Pahl, K. Derr, G. Gabel, I. Hinterseher, J.R. Elmore, C.M. Schworer, T. C. Peeler, D.P. Franklin, J.L. Gray, D.J. Carey, G. Tromp, H. Kuivaniemi, MicroRNA expression signature in human abdominal aortic aneurysms, BMC Med Genomics 5 (2012) 25.
[33] A. Torres-Do Rego, M. Barrientos, A. Ortega-Hernandez, J. Modrego, R. Gomez-Gordo, L.A. Alvarez-Sala, V. Cachofeiro, D. Gomez-Garre, Identification of a plasma microrna signature as biomarker of subaneurysmal aortic dilation in patients with high cardiovascular risk, J. Clin. Med. 9 (9) (2020).
[34] H. Zhou, F. Sun, M. Ou, Y. Zhang, M. Lin, L. Song, Y. Yu, H. Liao, W. Fan, H. Xing, M. Li, K. Zhao, X. Wu, Y. Sun, C. Liang, Y. Cai, L. Cui, Prior nasal delivery of antagomiR-122 prevents radiation-induced brain injury, Mol. Ther. 29 (12) (2021) 3465–3483.
[35] L. Zhang, H. Peng, W. Zhang, Y. Li, L. Liu, T. Leng, Yeast cell wall particle mediated nanotube-RNA delivery system loaded with miR365 antagomir for post-traumatic osteoarthritis therapy via oral route, Theranostics 10 (19) (2020) 8479–8493.
[36] I.R. Mordi, R.O. Forsythe, C. Gellatly, Z. Iskandar, O.M. McBride, A. Saratzis, R. Chalmers, C. Chin, M.J. Bown, D.E. Newby, C.C. Lang, J.T.J. Huang, A.M. Choy, Plasma desmosine and abdominal aortic aneurysm disease, J. Am. Heart Assoc. 8 (20) (2019) e013743.
[37] I. Mylonaki, É. Allémann, F. Saucy, J.A. Haefliger, F. Delie, O. Jordan, Perivascular medical devices and drug delivery systems: making the right choices, Biomaterials 128 (2017) 56–68.
[38] T. Shirasu, N. Yodsanit, J. Li, Y. Huang, X. Xie, R. Tang, Q. Wang, M. Zhang, G. Urabe, A. Webb, Y. Wang, X. Wang, R. Xie, B. Wang, K.C. Kent, S. Gong, L. W. Guo, Neointima abating and endothelium preserving - an adventitia-localized nanoformulation to inhibit the epigenetic writer DOT1L, Biomaterials 301 (2023) 122245.
[39] J. Yang, L. Rong, W. Huang, Z. Wu, Q. Ding, H. Zhang, Y. Lin, F. Li, C. Li, B.R. Yang, K. Tao, J. Wu, Flame-retardant, flexible, and breathable smart humidity sensing fabrics based on hydrogels for respiratory monitoring and non-contact sensing, View 4 (4) (2023).
[40] Z. Li, Y. Zhou, T. Li, J. Zhang, H. Tian, Stimuli-responsive hydrogels: fabrication and biomedical applications, View 3 (2) (2021).
[41] J.A. van Dongen, V. Getova, L.A. Brouwer, G.R. Liguori, P.K. Sharma, H.P. Stevens, B. van der Lei, M.C. Harmsen, Adipose tissue-derived extracellular matrix hydrogels as a release platform for secreted paracrine factors, Journal of tissue engineering and regenerative medicine 13 (6) (2019) 973–985.
[42] H. Che, Y. Wang, Y. Li, J. Lv, H. Li, Y. Liu, R. Dong, Y. Sun, X. Xu, J. Zhao, L. Wang, Inhibition of microRNA-150-5p alleviates cardiac inflammation and fibrosis via targeting Smad7 in high glucose-treated cardiac fibroblasts, J. Cell. Physiol. 235 (11) (2020) 7769–7779.
[43] C. Yuan, L. Ni, C. Zhang, X. Wu, The role of Notch3 signaling in kidney disease, Oxid. Med. Cell. Longev. 2020 (2020) 1809408.
[44] J.T. Baeten, B. Lilly, Notch signaling in vascular smooth muscle cells, Adv. Pharmacol. 78 (2017) 351–382.
[45] V. Domenga, P. Fardoux, P. Lacombe, M. Monet, J. Maciazek, L.T. Krebs, B. Klonjkowski, E. Berrou, M. Mericskay, Z. Li, E. Tournier-Lasserve, T. Gridley, A. Joutel, Notch3 is required for arterial identity and maturation of vascular smooth muscle cells, Genes Dev. 18 (22) (2004) 2730–2735.
[46] E. Biros, P.J. Walker, M. Nataatmadja, M. West, J. Golledge, Downregulation of transforming growth factor, beta receptor 2 and Notch signaling pathway in human abdominal aortic aneurysm, Atherosclerosis 221 (2) (2012) 383–386.
[47] P. Kavvadas, Z. Keuylian, N. Prakoura, S. Placier, A. Dorison, C.E. Chadjichristos, J. C. Dussaule, C. Chatziantoniou, Notch3 orchestrates epithelial and inflammatory responses to promote acute kidney injury, Kidney Int. 94 (1) (2018) 126–138.